Core–Shell Structures

DOI: 10.1002/anie.201406856

One-Nanometer-Precision Control of Al_2O_3 Nanoshells through a Solution-Based Synthesis Route**

Wei Zhang, Zi-Xiang Chi, Wen-Xin Mao, Rong-Wen Lv, An-Min Cao, and Li-Jun Wan**

Abstract: *Forming uniform metal oxide nanocoatings is a well-known challenge in the construction of core–shell type nanomaterials. Herein, by using buffer solution as a specific reaction medium, we demonstrate the possibility to grow thin nanoshells of metal oxides, typically Al_2O_3, on different kinds of core materials, forming a uniform surface-coating layer with thicknesses achieving one nanometer precision. The application of this methodology for the surface modification of $LiCoO_2$ shows that a thin nanoshell of Al_2O_3 can be readily tuned on the surface for an optimized battery performance.*

Core–shell structures have attracted a great deal of interest due to their versatility in regulating different components toward diverse applications such as catalysis, biology, energy conversion, and energy storage.[1] Typically, composite materials with a silica nanoshell have been developed to combine the advantages of both the silica shell and the core in benefit of the easy formation of silica shells.[2] The synthetic protocol developed by Stöber et al.[3] provides the ideal environment for slow hydrolysis and condensation of the silica precursor, usually silicon alkoxides, resulting in a heterogeneous nucleation and growth path.

Despite the success of silica coatings, it still remains a challenge to form metal oxide nanoshells, which is probably due to the high activity of the corresponding metal alkoxides.[4] The fast hydrolysis of these precursors favors either a homogenous nucleation process to form independent particles or a very thick coating layer on the substrate material.[5] Accordingly, the construction of uniform metal oxide nanoshells becomes even more challenging if a very thin surface layer, typically thinner than 5 nm, is necessary for designated functions.[6] For example, the coating effect is highly size-sensitive in different application areas such as shell-isolated nanoparticle-enhanced Raman spectroscopy (SHINERS),[6d] catalysis,[1a] and lithium-ion batteries.[6b]

We have paid special interest to the construction of a uniform nanoshell of Al_2O_3, which is an important metal oxide and has a wide range of applications, e.g., in catalysis,[1a,6f] optics,[6d] and energy conversion and storage.[7] Taking lithium-ion batteries as an example, surface modification by Al_2O_3 has been known as an indispensable step to treat different types of cathode materials, typically $LiCoO_2$.[8] Surface modification by Al_2O_3 can contribute in different ways such as alleviating the side reactions from the electrolytes[9] and improving the structural and cycle stabilities of $LiCoO_2$.[10] Unfortunately, the conventional Al_2O_3 coating methods such as aluminum alkoxide hydrolysis[11] cannot avoid the fast nucleation of $Al(OH)_3$, usually forming separate Al_2O_3 particles instead of a core–shell structure. Several groups have tried to circumvent this synthesis hurdle by utilizing the technique of atomic layer deposition (ALD),[6a,12] which can deposit Al_2O_3 layers onto the compressed cathode films at an atomic-scale precision. However, the ALD procedure is known to be very expensive and also very slow and tedious. It is of great importance to develop new synthetic protocols for growing Al_2O_3 nanoshells, which should be simple and easy, and also economic to scale up to deal with a large amount of powders with precise surface control.

In this contribution, we report our progress on the solution-based synthesis of uniform Al_2O_3 nanoshells on various core materials. For the first time, we demonstrate that the formation of Al_2O_3 nanoshells can be perfectly controlled in a buffer solution of formic acid/ammonium formate, which provides a suitable environment for manipulating the growth of aluminum hydroxide within one nanometer precision. Our preliminary results on the structure control of $LiCoO_2@Al_2O_3$ show that its battery performance is closely related to the shell thickness of Al_2O_3 and 1–2 nm coating layers show the best cyclability.

Briefly, a buffer solution of ammonium formate and formic acid was prepared and then the seed material of SnO_2 and the aluminum source $[Al_2(SO_4)_3]$ were added (a detailed procedure can be found in the Supporting Information, SI). After reaction, the solid sample was collected and heated at 450 °C for 2 h to yield the final product $SnO_2@Al_2O_3$ (SnO_2 core, Al_2O_3 shell). Figure 1a shows a typical transmission electron microscopy (TEM) image of the pristine SnO_2 nanoparticles (NPs). The high resolution TEM (HRTEM) image of a randomly selected particle reveals that it is highly crystalline with a free surface borderline (inset in Figure 1a). We find that a low concentration of $Al_2(SO_4)_3$ at 0.9 mM is effective to introduce a coating layer on the SnO_2 seeds. As

[*] W. Zhang, Z.-X. Chi, W.-X. Mao, Prof. A.-M. Cao, Prof. L.-J. Wan
Key Laboratory of Molecular Nanostructure and Nanotechnology and Beijing National Laboratory for Molecular Sciences
Institute of Chemistry, Chinese Academy of Sciences (CAS)
Beijing 100190 (China)
E-mail: anmin_cao@iccas.ac.cn
wanlijun@iccas.ac.cn
W.-X. Mao, Prof. R.-W. Lv
State Key Laboratory of Fine Chemicals
Dalian University of Technology
Dalian (China)

[**] This work was supported by the National Basic Research Program of China (2013CB934000 and 2013AA030803), the National Natural Science Foundation of China (21373238), and the Chinese Academy of Sciences.

Supporting information for this article is available on the WWW under http://dx.doi.org/10.1002/anie.201406856.

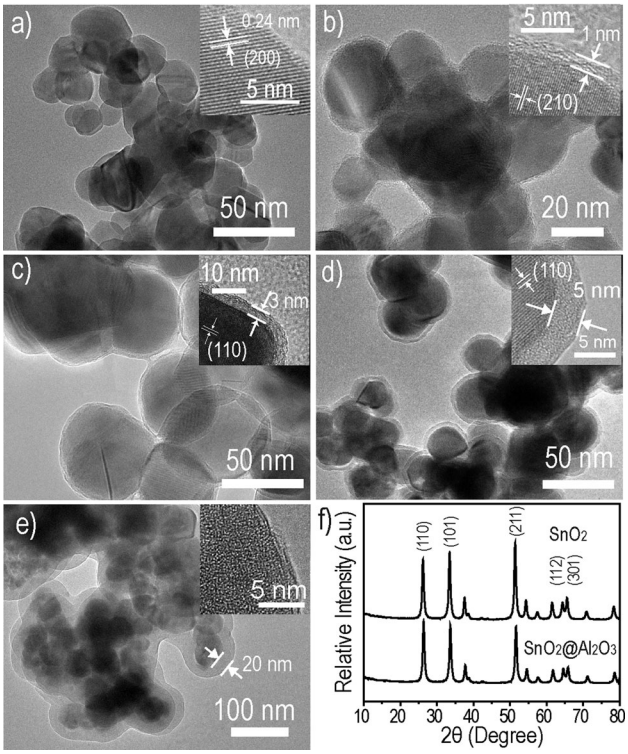

Figure 1. TEM (a–e) and XRD (f) characterization of the SnO_2@Al_2O_3 core–shell structured samples with different coating thickness: a) the pristine SnO_2, b–e) Al_2O_3 coating layers with thickness of 1 nm (b), 3 nm (c), 5 nm (d), and 20 nm (e). The insets in each picture are the corresponding HRTEM images of a randomly picked particle in the tested sample, showing the amorphous nature of the surface shell. f) XRD patterns of SnO_2 NPs and SnO_2@20 nm Al_2O_3. No peaks can be identified for Al_2O_3 and due to its amorphous nature.

shown in Figure 1 b, a very thin but still TEM-discernible shell distributes continuously and uniformly around all the SnO_2 surfaces. The HRTEM image shows that such a nanoshell has a thickness around 1 nm (inset in Figure 1 b). We found that an increase of the $Al_2(SO_4)_3$ concentration to 1.8 mM can produce a thicker coating layer as shown in Figure 1 c. The HRTEM image (inset in Figure 1 c) confirms that the resulting shell is 3 nm thick and is evenly distributed around the SnO_2 nanoparticles. As for 3.6 mM $Al_2(SO_4)_3$, the nanoshell becomes much more evident as shown in Figure 1 d). For this newly emerged surface layer, no obvious lattice fringe can be identified in the TEM image and the X-ray diffraction (XRD) pattern shows no additional peaks (Figure 1 f), indicating the amorphous nature of the surface shell. For a pure Al_2O_3 sample, which is synthesized without SnO_2 seeds added to the same buffer solution, the XRD characterization also reveals that the newly precipitated Al_2O_3 is amorphous unless being heated at a very high temperature (Figure S1). X-ray photoelectron spectroscopy (XPS) reveals the emergence of Al and O after coating (Figure S2), verifying the formation of an Al_2O_3 shell. A further increase of the concentration of $Al_2(SO_4)_3$ to 12 mM forms a 20 nm Al_2O_3 coating layer (Figure 1 e). No obvious phase separation can be identified according to our scanning electronic microscopy investigation (Figure S3).

Our further investigation shows that the Al_2O_3 nanoshell grows in a stepwise manner as the reaction proceeds. Time-dependent experiments have been carried out to track the growth of a 5 nm Al_2O_3 nanoshell shown in Figure 1 d. The samples were collected at different reaction stages and then subjected to TEM characterization. The shell was 1 nm in thickness if the reaction lasts for only 15 min (Figure S4a). After another 15 min reaction, it is increased to 3 nm (Figure S4b). The shell continues to grow and 30 min later a thickness of 4 nm is reached (Figure S4c). The coating reaction gradually slows down and is finished after 2 h as shown by the unchanged thickness thereafter (Figure S4d). Through the control of the reactant concentrations and the reaction time, we are able to coat the SnO_2 NPs with uniform Al_2O_3 shells and can also conveniently tune the shell thickness in a nanometer-by-nanometer way.

For the formation of core–shell structures, the lattice mismatch between the core and the shell has been known as a tremendous obstacle for surface coating due to the substantial interfacial tension.[1e,5b] The creation of an amorphous shell instead of a crystalline one becomes a more favorable choice as is evident by a large number of core–shell structures constructed by amorphous silica.[2] Similarly, the formation of an amorphous Al_2O_3 shell makes the synthetic protocol very easy to be applied to different kinds of substrates. Representative materials, including metals, metal oxides, and nonmetals, were selected as core materials as shown in Figure 2. Systematic control of the coating thickness

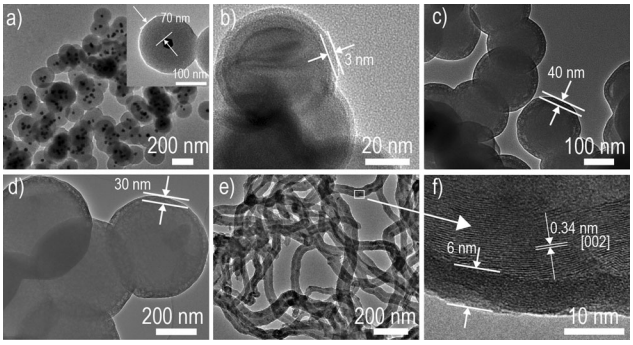

Figure 2. TEM images of core–shell structures synthesized with different seeds: a) 35 nm Au@70 nm Al_2O_3, the TEM image of Au is shown in Figure S5, b) 60 nm Si@3 nm Al_2O_3, c) 160 nm SiO_2@40 nm Al_2O_3, d) 460 nm PS@30 nm Al_2O_3, e) 35 nm MWCNT@6 nm Al_2O_3, f) HRTEM image of 35 nm MWCNT@6 nm Al_2O_3.

can also be achieved through a concerted control of the reaction time and the reactant concentrations. Despite the big difference in these substrates, which ranges from metal (Au, Figure 2 a) to metalloid (Si, Figure 2 b), and then to nonmetal oxide (SiO_2, Figure 2 c), the amorphous Al_2O_3 can anchor right on the surface of the core materials, forming a uniform coating layer.

Further experiments show that it is also possible to coat organic substrates with Al_2O_3 and the hollow Al_2O_3 structure

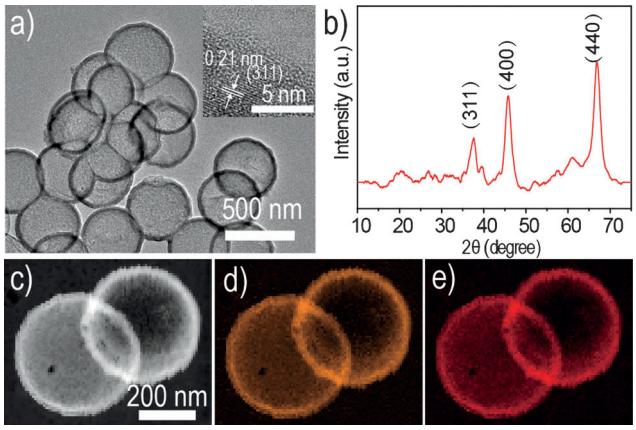

Figure 3. a) TEM image of hollow Al_2O_3 nanospheres after the PS core has been removed, inset shows the lattice fringe of the shell. b) XRD pattern for samples after high-temperature treatment. c–e) STEM characterization of two representative nanospheres: c) morphology mode of STEM image, d,e) elemental mappings of Al (d) and O (e) on these two particles.

can be subsequently created by burning off the cores. For example, polystyrene nanoparticles can firstly be coated with an Al_2O_3 surface layer and form a uniform core shell structure of PS@Al_2O_3 (Figure 2c). A following heat treatment in air at a temperature as high as 900°C can not only remove the central organic cores to create a cavity (Figure 3a), but can also convert the amorphous Al_2O_3 into a crystalline phase. As shown in Figure 3b, the characteristic XRD peaks of γ-Al_2O_3 (JCPDS no. 29-0063) emerges after the high-temperature treatment. A thorough morphology examination on TEM (Figure 3a, Figure S6) and SEM images (Figure S7) shows that all the particles are hollow and no separate solid Al_2O_3 nanospheres exist. Two hollow Al_2O_3 nanospheres have been randomly picked and their morphology was examined by scanning TEM (STEM, Figure 3c). The elemental mapping is also carried out as shown in Figure 3c,d. Both Al and O can be clearly identified in each particle and the brighter edge is in good agreement with the hollow characteristics. It's also easy to tune the shell thickness of these hollow structures as shown in Figure S6. It notes that all these particles show almost identical shape with an evenly-distributed surface layer, demonstrating the advantage of the buffer solution for the formation of uniform nanoshells.

In addition to the spherical particles mentioned above, it is also convenient to coat core materials of different shapes. For example, using multiwalled carbon nanotubes (MWCNT) as seed materials, we are able to prepare the core–shell structure of MWCNT@Al_2O_3 as shown in Figure 2e. The HRTEM image (Figure 2f) confirms the existence of a continuous Al_2O_3 surface layer on the crystalline carbon nanotube. Similar to PS@Al_2O_3, Al_2O_3 nanotubes can be prepared after the removal of the central MWCNT (Figure S8a) as identified by the detailed STEM characterization (Figure S8b–d).

According to the LaMer's law,[13] to achieve a slow heterogeneous growth rather than self-nucleating into separate particles, the growth kinetics of the precipitate has to be under control so that a balance between nucleation and growth can be achieved. Our synthesis reveals that the use of buffer solution can be a simple but very effective route to achieve this goal. For comparison, ammonia-induced precipitation[14] is easy to form separate Al_2O_3 particles as shown in Figure S9a. The quick interaction between ammonia and Al^{3+} results in a burst of nuclei, accordingly forming $Al(OH)_3$ particles instead of a surface shell. The advantage of buffer solution can be further demonstrated by a control test in which only a formic acid solution was used as the reaction medium instead of the buffered one. For the formic acid solution, although it is easy to start the reaction from the desired pH (4.4), the pH would drop during heating and it turned out that no obvious coating layer could be achieved as shown in Figure S9b.

For the formation of a decent Al_2O_3 shell, we found that a pH range between 3.8 and 4.6 should be guaranteed for the buffer solution as shown in Scheme 1. To precipitate the Al^{3+}, a certain concentration of hydroxy groups should be provided

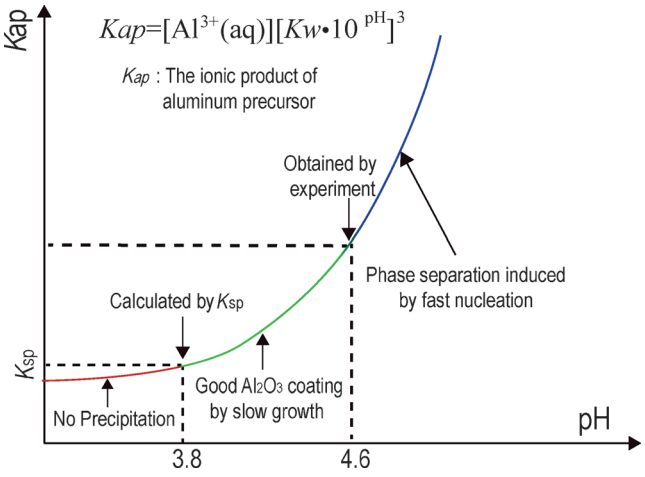

Scheme 1. Diagram of the relationship between the ionic product of the aluminum precursor (K_{ap}) and the pH. The line falls into three different segments highlighted in different colors. Red: no $Al(OH)_3$ precipitation for pH lower than 3.8; blue: separate $Al(OH)_3$ particles for pH higher than 4.6; green: heterogeneous growth of $Al(OH)_3$ for a pH range between 3.8 and 4.6.

so that the ionic product of the aluminum precursor (K_{ap}) can be higher than the solubility constant (K_{sp}), otherwise no $Al(OH)_3$ can form because its saturation point won't be reached. A quick calculation based on the chemical equilibria involved in the formation of $Al(OH)_3$ (Scheme S1) determines a minimum pH value of 3.8, at which K_{ap} equals K_{sp} for this 3.2 mM $Al_2(SO_4)_3$. Accordingly, no precipitation occurred in a more acidic buffer solution at pH 3.4 (Figure S9c). It is worthwhile noting that the formic acid/ammonium formate buffer solution is a logical choice in our synthesis design. The pK_a value of formic acid is 3.8[15] so that the formic acid/ammonium formate combination can have a good buffering range between 2.8 and 4.8. Due to the good balance between formic acid and formate ions, no obvious pH change has been observed during our coating process, indicating a stable

provision of hydroxide groups for $Al(OH)_3$ formation. However, when the pH value is too high, for example, 5.4 from the acetic acid and ammonium acetate buffer solution, we observe an obvious phase separation between $Al(OH)_3$ and SnO_2 (Figure S9d), probably due to the fast nucleation speed caused by the high concentration of hydroxy groups. Our synthesis efforts showed that a pH range between 3.8 and 4.6 can give appropriate K_{ap} values suitable for $Al(OH)_3$ coating.

We found that buffer solutions other than the formic acid/ammonium formate one can also be able to produce Al_2O_3 coatings as long as an appropriate buffer range was guaranteed. For example, aspartic acid has a pK_a value of 3.7[15] and the pair of aspartic acid/aspartate can provide a decent buffering capability around pH 4.0. Similarly, a very thin Al_2O_3 nanoshell was also successfully achieved by means of this buffer solution as shown in Figure S10. Moreover, due to the good control of OH^- concentration in benefit of a variety of buffer solutions, it also becomes possible to form metal oxide nanoshells other than Al_2O_3. Our preliminary trials showed that this synthesis protocol based on buffer solution could also be readily expanded to form nanoshells of different metal oxides such as ZrO_2 and ZnO as shown in Figure S11.

The good control on the formation of Al_2O_3 nanoshells endows us the capability to carry out delicate surface modification on cathode materials of LIBs with a nanometer precision, which has always been considered as a privilege of the ALD technique.[16] Taking $LiCoO_2$ as an example, for the first time, it becomes possible to deposit Al_2O_3 on a large amount of $LiCoO_2$ powder (Figure S12) nanometer by nanometer through a solution-based route. Figure 4 a–d shows the TEM images of different surface-modified $LiCoO_2$ samples. When a very low $Al_2(SO_4)_3$ concentration is used in the buffer solution, it turns out to be difficult to form a uniform coating layer on the pristine $LiCoO_2$ and only discontinuous islands can be observed on the surface (Figure 4 a). For increased $Al_2(SO_4)_3$ concentrations, we are able to form continuous and uniform Al_2O_3 coating layers with thickness controlled at 1 nm, 2 nm, 3 nm. The content of Al_2O_3 in these samples were determined by inductively coupled plasma atomic emission spectroscopy (ICP-AES) as shown in Table S1.

Such a precise control of the surface coating of $LiCoO_2$ enabled us to optimize its battery performance by tuning the thickness of Al_2O_3 nanoshells. A high working voltage at 4.5 V is tested not only because it is an ongoing pursuit for higher energy density, but also due to the fact that the increased instability in battery performance can reveal the surface contribution. Figure 4 e shows the charge/discharge profiles of different samples we tested. A characteristic plateau at 4.2 V can be observed due to the phase transfer of $LiCoO_2$ from monoclinic to hexagonal. A thick Al_2O_3 layer at 3 nm shows an apparent polarization in the charge/discharge curve, probably due to the low conductivity of the coating layer.[6a] On the contrary, thinner layers of 1 nm and 2 nm do not show an obvious polarization. These can be further confirmed by the cyclic voltammetry measurement as shown in Figure S13. Importantly, as shown in Figure 4 f, a uniform coating with the thickness at 1 nm shows the best cyclability at a current density of 18 mA g^{-1}. Considering that the Al_2O_3 does not change the structure of the pristine $LiCoO_2$ (Figure S14), the surface Al_2O_3 mainly contributes as a protection layer during cycling as reported by different groups.[8a,9,12a,17] An optimal protection turns out to be a compromise between surface protection and polarization: a discontinuous surface coating cannot provide a good protection, whereas polarization prevails for a too thick coating. Detailed characterizations by using electrochemical impedance spectroscopy (EIS) showed an increased charge-transfer resistance (R_{ct}) and a much higher surface film resistance (R_f) for the sample with a 3 nm coating layer (Figure S15, Table S2) compared with those samples with thinner coatings, showing a trend in good agreement with their battery performance.

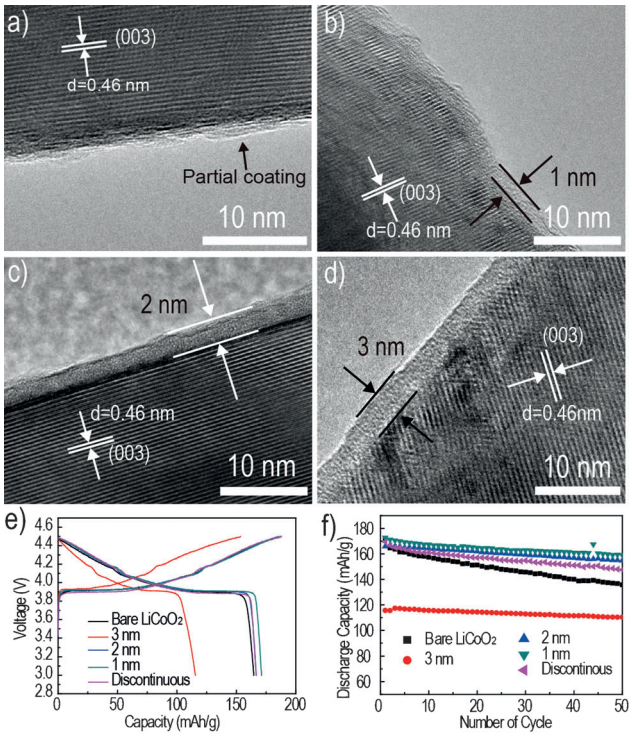

Figure 4. a–d) TEM images of surface-modified $LiCoO_2$ samples with different shell thickness: a) discontinuous Al_2O_3 for a partial coverage, b) 1 nm Al_2O_3, c) 2 nm Al_2O_3, d) 3 nm Al_2O_3; e,f) electrochemical performance of the above-mentioned samples: e) charge/discharge profiles, and f) cycling performance. The data is collected at 0.1 C and the working voltage is between 3.0 V and 4.5 V.

In summary, a synthetic protocol based on buffer solution is developed for the coating of Al_2O_3 nanoshells onto different kinds of substrates. Benefiting from the stable environment provided by a suitable buffer solution, the growth of Al_2O_3 can be readily controlled, leading to the formation of uniform nanoshells with precisely defined thickness with up to one nanometer precision. By means of the accurate surface modification, good model systems can be built to optimize the coating effects. Our preliminary results on the surface control of $LiCoO_2$ show the close relationship between the battery performance and its surface Al_2O_3 coating layers. A uniform shell with a thickness around 1–

2 nm shows the best cyclability probably due to the balance between polarization and surface protection.

Received: March 7, 2014
Revised: August 18, 2014
Published online: October 21, 2014

Keywords: Al_2O_3 coating · core–shell structure · layer thickness · lithium-ion batteries

[1] a) M. Cargnello, J. J. Delgado Jaen, J. C. Hernandez Garrido, K. Bakhmutsky, T. Montini, J. J. Calvino Gamez, R. J. Gorte, P. Fornasiero, *Science* **2012**, *337*, 713 – 717; b) N. Lee, H. R. Cho, M. H. Oh, S. H. Lee, K. Kim, B. H. Kim, K. Shin, T. Y. Ahn, J. W. Choi, Y. W. Kim, S. H. Choi, T. Hyeon, *J. Am. Chem. Soc.* **2012**, *134*, 10309 – 10312; c) O. Chen, J. Zhao, V. P. Chauhan, J. Cui, C. Wong, D. K. Harris, H. Wei, H.-S. Han, D. Fukumura, R. K. Jain, *Nat. Mater.* **2013**, *12*, 445 – 451; d) J. Tang, Z. Huo, S. Brittman, H. Gao, P. Yang, *Nat. Nanotechnol.* **2011**, *6*, 568 – 572; e) J. Zhang, Y. Tang, K. Lee, M. Ouyang, *Science* **2010**, *327*, 1634 – 1638; f) H. Wu, G. Chan, J. W. Choi, I. Ryu, Y. Yao, M. T. McDowell, S. W. Lee, A. Jackson, Y. Yang, L. Hu, *Nat. Nanotechnol.* **2012**, *7*, 310 – 315; g) K. T. Lee, S. Jeong, J. Cho, *Acc. Chem. Res.* **2013**, *46*, 1161 – 1170; h) R. Ghosh Chaudhuri, S. Paria, *Chem. Rev.* **2012**, *112*, 2373 – 2433.

[2] J. Kim, H. S. Kim, N. Lee, T. Kim, H. Kim, T. Yu, I. C. Song, W. K. Moon, T. Hyeon, *Angew. Chem. Int. Ed.* **2008**, *47*, 8438 – 8441; *Angew. Chem.* **2008**, *120*, 8566 – 8569.

[3] W. Stöber, A. Fink, E. Bohn, *J. Colloid Interface Sci.* **1968**, *26*, 62 – 69.

[4] B. Wu, C. Guo, N. Zheng, Z. Xie, G. D. Stucky, *J. Am. Chem. Soc.* **2008**, *130*, 17563 – 17567.

[5] a) W. Li, J. Yang, Z. Wu, J. Wang, B. Li, S. Feng, Y. Deng, F. Zhang, D. Zhao, *J. Am. Chem. Soc.* **2012**, *134*, 11864 – 11867; b) H. Sun, J. He, J. Wang, S.-Y. Zhang, C. Liu, T. Sritharan, S. Mhaisalkar, M.-Y. Han, D. Wang, H. Chen, *J. Am. Chem. Soc.* **2013**, *135*, 9099 – 9110.

[6] a) Y. S. Jung, A. S. Cavanagh, A. C. Dillon, M. D. Groner, S. M. George, S.-H. Lee, *J. Electrochem. Soc.* **2010**, *157*, A75 – 81; b) S. Sim, P. Oh, S. Park, J. Cho, *Adv. Mater.* **2013**, *25*, 4498 – 4503; c) V. Uzayisenga, X. D. Lin, L. M. Li, J. R. Anema, Z. L. Yang, Y. F. Huang, H. X. Lin, S. B. Li, J. F. Li, Z. Q. Tian, *Langmuir* **2012**, *28*, 9140 – 9146; d) J. F. Li, Y. F. Huang, Y. Ding, Z. L. Yang, S. B. Li, X. S. Zhou, F. R. Fan, W. Zhang, Z. Y. Zhou, D. Y. Wu, *Nature* **2010**, *464*, 392 – 395; e) J. Oliver-Meseguer, J. R. Cabrero-Antonino, I. Dominguez, A. Leyva-Perez, A. Corma, *Science* **2012**, *338*, 1452 – 1455; f) J. Lu, B. Fu, M. C. Kung, G. Xiao, J. W. Elam, H. H. Kung, P. C. Stair, *Science* **2012**, *335*, 1205 – 1208.

[7] a) E. Palomares, J. N. Clifford, S. A. Haque, T. Lutz, J. R. Durrant, *Chem. Commun.* **2002**, 1464 – 1465; b) F. Fabregat-Santiago, J. García-Cañadas, E. Palomares, J. N. Clifford, S. A. Haque, J. R. Durrant, G. Garcia-Belmonte, J. Bisquert, *J. Appl. Phys.* **2004**, *96*, 6903 – 6907.

[8] a) Z. Wang, L. Liu, L. Chen, X. Huang, *Solid State Ionics* **2002**, *148*, 335 – 342; b) J. B. Goodenough, K. S. Park, *J. Am. Chem. Soc.* **2013**, *135*, 1167 – 1176.

[9] I. D. Scott, Y. S. Jung, A. S. Cavanagh, Y. Yan, A. C. Dillon, S. M. George, S. H. Lee, *Nano Lett.* **2011**, *11*, 414 – 418.

[10] K. T. Lee, S. Jeong, J. Cho, *Acc. Chem. Res.* **2012**, *46*, 1161 – 1170.

[11] Y. J. Kim, J. Cho, T.-J. Kim, B. Park, *J. Electrochem. Soc.* **2003**, *150*, A1723 – 1725.

[12] a) Y. S. Jung, A. S. Cavanagh, L. A. Riley, S. H. Kang, A. C. Dillon, M. D. Groner, S. M. George, S. H. Lee, *Adv. Mater.* **2010**, *22*, 2172 – 2176; b) Y. He, X. Yu, Y. Wang, H. Li, X. Huang, *Adv. Mater.* **2011**, *23*, 4938 – 4941; c) X. Han, Y. Liu, Z. Jia, Y.-C. Chen, J. Wan, N. Weadock, K. J. Gaskell, T. Li, L. Hu, *Nano Lett.* **2014**, *14*, 139 – 147.

[13] V. K. LaMer, R. H. Dinegar, *J. Am. Chem. Soc.* **1950**, *72*, 4847 – 4854.

[14] W.-K. Kim, D.-W. Han, W.-H. Ryu, S.-J. Lim, H.-S. Kwon, *Electrochim. Acta* **2012**, *71*, 17 – 21.

[15] J. G. Speight, *Lange's handbook of chemistry*, *Vol. 1*, McGraw-Hill, New York, **2005**.

[16] M. Leskelä, M. Ritala, *Angew. Chem. Int. Ed.* **2003**, *42*, 5548 – 5554; *Angew. Chem.* **2003**, *115*, 5706 – 5713.

[17] J. Cho, T.-J. Kim, B. Park, *J. Electrochem. Soc.* **2002**, *149*, A288 – 292.

